

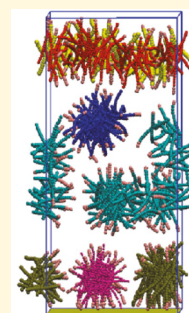
Adsorption and Self-Assembly of Surfactants on Metal–Water Interfaces

Xueying Ko¹ and Sumit Sharma*¹

Department of Chemical and Biomolecular Engineering, Ohio University, Athens, Ohio 45701, United States

Supporting Information

ABSTRACT: Modifying properties of metal–water interfaces via adsorption of surfactants has applications in electrochemistry and catalysis. We report molecular simulations of adsorption of surfactant molecules on metal surfaces wherein we systematically vary the strength of hydrophobic interaction between surfactant tails, as well as the size of the surfactants' polar head group. A surfactant molecule is represented by a linear, bead–spring model with a polar “head” bead and a chain of hydrophobic “tail” beads. A smooth surface, strongly attractive to the polar beads, represents the metal surface. Our main findings are that (1) hydrophobic interactions between adsorbed molecules promote adsorption and self-assembly and (2) the morphology of the adsorbed layer is governed by the geometry of the molecules. When the size of the polar bead is the same as that of the hydrophobic beads, an adsorbed self-assembled monolayer (SAM) is formed. When the polar bead is larger than the hydrophobic beads, cylindrical micelles are formed in the bulk and the adsorbed phase. For the adsorbed SAM, the layer is patchy, with a significant fraction of the molecules adsorbed with their polar beads pointing away from the surface. These results corroborate with experimental observations and provide new insights into the molecular nature of adsorbed layers.



INTRODUCTION

Metal–water interfaces are ubiquitous in heterogeneous catalysis¹ and electrochemical reactions.² The ability to adjust properties of these interfaces via adsorption of surfactants has found applications in corrosion inhibition,³ electrochemistry,⁴ biomimetic design,⁵ fuel cells,⁶ and energy storage.⁷ The direct application that we are interested in is the use of surfactants as inhibitors of aqueous corrosion of metals in oil and gas pipelines. Organic, surface-active amphiphilic molecules have been found to be effective corrosion inhibitors.^{3,8,9} These molecules contain both hydrophobic (nonpolar “tail”) and hydrophilic (polar “head”) groups. The hydrophobic tails are long hydrocarbon chains (usually C6–C22), while hydrophilic heads are either nonionic or ionic functional groups. Imidazole, quaternary ammonium, amide, and amido-amine based surfactants are popular corrosion inhibitors because of their low toxicity and high efficacy.^{9–11} Due to their amphiphilic nature, these molecules adsorb onto metal–water interfaces and alter the nature of electrochemical reactions.¹² However, the performance of these compounds is found to vary with operating conditions, leading to unpredictable behavior and many corrosion-related failures.^{3,13} Hence, there is a need to design new inhibitor molecules with well-understood and robust corrosion mitigation capabilities under varying conditions. So far, this pursuit has largely relied on trial and error experimentation^{3,14–17} because a fundamental understanding of the relationship between adsorption characteristics and molecular properties of surfactant molecules has been lacking.

Adsorption of surfactant molecules on hydrophobic surfaces is mainly driven by hydrophobic interactions between the alkyl tails and between the alkyl tails and the surface.^{18,19} As a result, hemicylindrical or hemispherical structures are observed in the

adsorbed phase.^{18,20} On polar surfaces, initial stages of adsorption of surfactants is driven by the affinity between the polar head groups and the surface and/or adsorbed counterions.^{21,22} In later stages, lateral hydrophobic interactions between the alkyl tails are understood to promote adsorption.^{21,22} The resulting adsorbed phases manifest many different morphologies, such as self-assembled layers or cylindrical or spherical micelles.^{4,23,24} Adsorption isotherms of quaternary ammonium-based surfactants are observed to shift toward lower concentrations with increase in alkyl tail lengths, highlighting the importance of hydrophobic interactions in promoting adsorption.^{25,26} On the other hand, equilibrium adsorbed concentrations of imidazoline-based surfactant molecules on metal–water interfaces have been reported to be invariant of the alkyl tail length.¹¹ These seemingly contrary results on the role of alkyl tails on adsorption have not been reconciled.

Alkyl tails of adsorbed surfactants are known to affect interfacial properties; for example, molecules with small alkyl tails (<C₆) show a significantly reduced corrosion inhibition efficiency.¹¹ The inability of small alkyl tails to form an effective hydrophobic barrier is often cited as the reason for these observations. For corrosion inhibition and electrochemistry applications, complete coverage of metal–water interfaces with surfactants is desired to achieve electrochemical “blocking”.^{4,8} The premise that adsorption is chiefly governed by the interaction between polar groups and the surface has prompted researchers to test surfactants with highly polar head groups

Received: September 18, 2017

Revised: October 26, 2017

Published: October 30, 2017

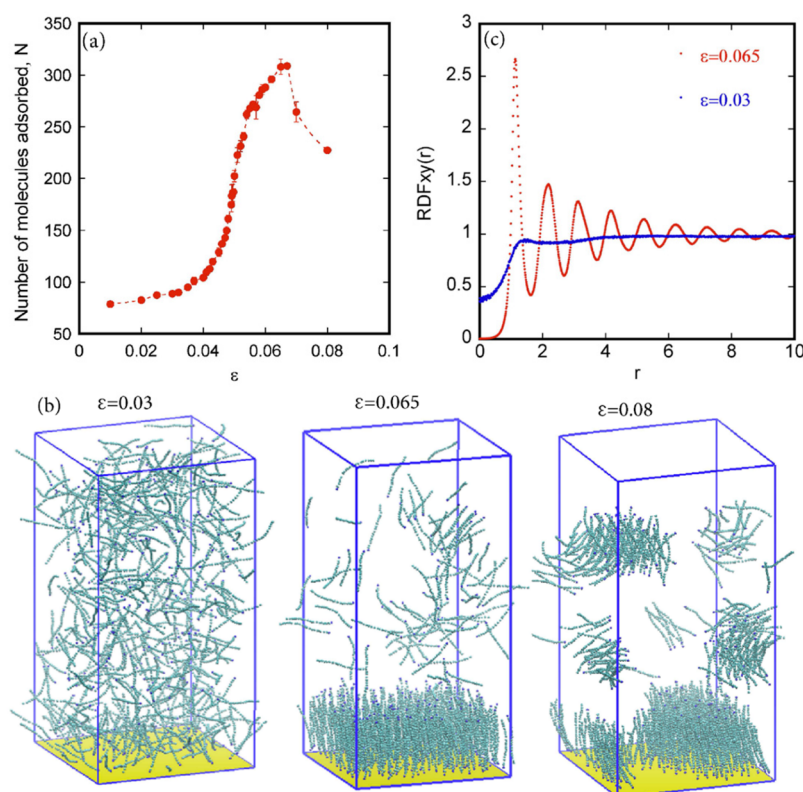


Figure 1. Adsorption behavior of surfactant molecules with $\sigma_p = \sigma$. (a) Number of adsorbed molecules, N , as a function of strength of hydrophobic interactions, ϵ . The molecules with their center of mass within a distance of 6σ from the surface are counted as adsorbed. This criterion is based on the observed density profile of the center of mass of the molecules as a function of the distance from the surface (Supporting Information Figure 1S). Error bars in this figure are standard deviations of ensemble averages calculated from 3 to 5 independent simulations. The line is a guide to the eye. (b) Snapshots of the system for $\epsilon = 0.03$ (low adsorption), $\epsilon = 0.065$ (self-assembled monolayer), and $\epsilon = 0.08$ (lamellar micelles in the bulk and on the surface). The surface is shown as a yellow plane. The molecules are shown as green (hydrophobic) and blue (polar) beads. (c) Radial distribution function of the center of mass of the adsorbed molecules in the XY plane for $\epsilon = 0.03$, which corresponds to the low adsorption regime, and $\epsilon = 0.065$, which corresponds to the adsorbed self-assembled monolayer.

comprising bulky heterocyclic and aromatic groups.³ However, little importance is given to understanding how the size of the polar head group impacts the nature of the adsorbed layer. Hence, there is a need to perform a systematic investigation of how different molecular features of surfactants affect their adsorption characteristics on metal–water interfaces.

In this work, we employ molecular simulations to understand how the hydrophobic character of the alkyl tail and the size of the polar head group of the surfactants affect their adsorption behavior on a metal surface. We find that tail hydrophobicity plays an important role in driving adsorption and self-assembly of surfactant molecules. The geometry of the molecule dictates the aggregation morphology in the adsorbed and the bulk phases.

METHODS

Simulation System. We use a coarse-grained bead–spring model to represent surfactant molecules. All quantities in the simulation system are defined in reduced units of energy, mass, and length, and therefore, the results can be translated into real units by appropriate conversions.²⁷ In this model, one terminal bead of a surfactant molecule is the polar head bead, and the remaining beads are hydrophobic and form the tail. The beads are connected via bonded interactions modeled as harmonic potentials centered at 0.3σ . The angles between adjacent bonds in a surfactant molecule are restrained via angular harmonic potentials centered at 180° . Water molecules are not modeled

explicitly. An effective attractive interaction between the hydrophobic tail beads incorporates the hydrophobic effect. This interaction is modeled as a Lennard-Jones (LJ) potential with the well-depth ϵ (arbitrary energy units) and the length parameter σ (arbitrary length units). The polar beads interact with all other beads via a purely repulsive Weeks–Chandler–Andersen (WCA) potential.²⁸ The WCA potential comprises only the repulsive part of the LJ potential. The basis of employing this potential is the understanding that the interactions of a polar group with water and with other polar and hydrophobic groups are similar in magnitude and length scale in an aqueous medium. As a result, there are no net attractive interactions between two polar groups or between a polar group and a hydrophobic group in an aqueous medium.²⁹ The surface is represented by a smooth wall at $Z = 0$. The strong affinity between the polar beads of the surfactant molecules and the surface is modeled by a 9–3 interaction potential with the well-depth parameter ϵ_s . The hydrophobic beads do not have attractive interactions with the surface. Reflective boundary conditions at $Z = 0$ are used to prevent the hydrophobic beads from crossing the surface. To keep the simulation volume constant, reflective boundary conditions are used for all beads for the face opposite the surface in the simulation box. The simulation box is periodic in the X and Y dimensions. The X and Y dimensions of the simulation box are kept fixed at $20\sigma \times 20\sigma$. The Z dimension (the dimension perpendicular to the surface) is chosen to ensure that the

number density of the beads in the system is maintained at $0.5\sigma^{-3}$. Hence, for 400 molecules of 20mers, the Z dimension is 40σ . The mass of each bead, m , is taken as 1 (arbitrary mass units).

Simulation Details. Langevin dynamics molecular simulations are performed at a fixed temperature of 1.0 (temperature units, $K_B T/\epsilon$) and a damping constant of 0.1 (time units, $(\epsilon/m\sigma^2)^{0.5}t$).²⁷ In order to study the role of hydrophobic character of the tails on adsorption, the LJ well-depth parameter for the interactions between the hydrophobic beads ϵ is varied from 0.01 to 0.11 in a series of simulations. The rationale behind choosing these values is that for $\epsilon = 0.05$, the total interaction energy between two surfactant molecules is $O(K_B T)$, in accordance with the observed potential of mean force between two ~ 1 nm sized hydrophobic solutes.³⁰ The well-depth of the interaction between the surface and the polar bead, ϵ_s , is kept at a fixed value of 5.0. This value is chosen to match the interaction energy obtained from density functional theory (DFT) calculations of polar groups on metal surfaces.³¹ The bond and angle harmonic potential coefficients are set to 100 (energy units/ σ^2) and 50 (energy units/radians²), respectively. Simulations of 20mer surfactant molecules are performed for different values of ϵ at a fixed monomer number density of $0.5\sigma^{-3}$ (a 20mer molecule has one polar head bead and 19 hydrophobic tail beads). To study the effect of the size of the polar head group, three different values of the polar bead's WCA length scale parameter, $\sigma_p = \sigma, 1.5\sigma$, and 2σ , are chosen. The WCA well-depth parameter, ϵ_p is kept fixed at 1.0. Along with these simulations, we also perform Langevin dynamics simulations in the bulk (that is, in the absence of a surface) in order to study bulk aggregation behavior. While we change the size of the polar beads, we do not change their mass. Hence, we keep the same damping constant of 0.1 (time units) in all of the simulations. All simulations are performed using the large-scale atomic/molecular massively parallel simulator (LAMMPS) MD simulations package.³² Typically, for each simulation, the system is first equilibrated for $3-8 \times 10^8$ MD steps with a time step of 0.001, followed by a production run of $8-16 \times 10^8$ MD steps. Equilibration is understood to be achieved when no change in the ensemble-averaged surface adsorbed amount, orientation factor (discussed below), and energy of the system is observed.

RESULTS AND DISCUSSION

Effect of Tail Hydrophobicity on Adsorption Behavior.

In the first set of simulations, the ϵ (the LJ well-depth parameter between hydrophobic beads) is varied from 0.01 to 0.09 while keeping all other parameters fixed and with $\sigma_p = \sigma$. The value of ϵ sets the strength of attractive interactions between the hydrophobic beads of the surfactant molecules. A small ϵ implies a weak attraction, whereas a large ϵ implies a strong attraction between the hydrophobic beads. By changing the value of ϵ , one can evaluate how the hydrophobic character of the tail affects the adsorption behavior. Figure 1a shows the number of adsorbed molecules as a function of ϵ . For small values of ϵ (< 0.04), that is, for weakly hydrophobic tails, low levels of adsorption are observed. Above $\epsilon = 0.04$, a sharp increase in equilibrium adsorption is seen, which reaches a maximum for $\epsilon = 0.065$. Beyond $\epsilon = 0.065$, a decrease in the equilibrium adsorption is seen. Figure 1b shows snapshots corresponding to three different ϵ values: (1) $\epsilon = 0.03$, (2) $\epsilon = 0.065$, and (3) $\epsilon = 0.08$. Clearly, for $\epsilon = 0.03$, the molecules adsorb in random orientations on the surface. For $\epsilon = 0.065$, a

self-assembled monolayer (SAM) in the adsorbed state is observed while the molecules in the bulk are randomly oriented. For $\epsilon = 0.08$, the molecules aggregate in both bulk and adsorbed phases as laminar micelles. Hence, as ϵ is increased from 0.04 to 0.065, making the tails more hydrophobic, the adsorption regime changes from low, random adsorption to an adsorbed SAM. Beyond $\epsilon = 0.065$, molecular aggregates are formed in the bulk, and the molecules do not diffuse toward the surface, thereby decreasing adsorption. Figure 1c shows the radial distribution function of the center of mass of the adsorbed molecules in the plane of the surface (the XY plane), $RDF_{xy}(r)$, for $\epsilon = 0.065$ and 0.03. The RDF_{xy} for $\epsilon = 0.03$ resembles that of a low-density phase with no local order, while for $\epsilon = 0.065$, the $RDF_{xy}(r)$ shows regular peaks corresponding to the ordered structure of the SAM. The gradually decreasing peaks indicate that the SAM is not a solid but has fluid-like behavior.

The adsorption behavior observed above can be understood by analyzing the orientation factor of the molecules on the surface and in the bulk as a function of ϵ (Figure 2). The

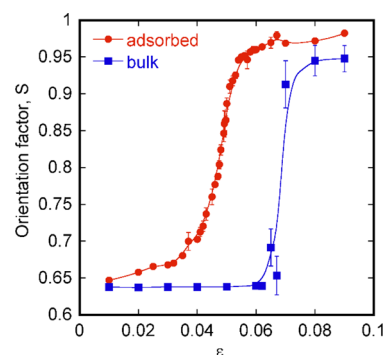


Figure 2. Orientation factor, S of molecules with $\sigma_p = \sigma$ in the bulk and the adsorbed phases as a function of strength of hydrophobic interactions, ϵ . A large value of S (~ 1) implies strong orientation of molecules parallel or antiparallel to each other. A small value of S (~ 0.5) corresponds to random orientation of the molecules with respect to each other. Error bars are standard deviations of ensemble averages calculated from 3–5 independent simulations. Lines are guides to the eye.

orientation factor, S , is defined as the largest eigenvalue of the tensor Q , the elements of which are given by³³

$$Q_{\alpha\beta} = \frac{1.5}{N_t} \sum_{i=1}^{N_t} |n_{i\alpha} \cdot n_{i\beta}| - \frac{1}{2} \delta_{\alpha\beta} \quad (1)$$

where $n_{i\alpha}$ and $n_{i\beta}$ are the α and β components of the end-to-end vector of the molecule i , respectively. $\delta_{\alpha\beta} = 1$ if $\alpha = \beta$ and 0 otherwise. N_t is the total number of molecules in the system. If all of the molecules are perfectly oriented parallel to each other, then $S = 1$. For a completely random orientation, $S = 0.5$.

Figure 2 shows S as a function of ϵ for bulk and adsorbed phases. For $\epsilon < 0.04$ (weakly hydrophobic tails), S is small in the adsorbed phase, indicating random orientation of the adsorbed molecules. For $\epsilon > 0.04$, a sharp increase in the value of S in the adsorbed phase is observed. This indicates that as ϵ increases the adsorbed molecules start aligning parallel (or antiparallel) to each other. For $\epsilon > 0.06$, S is close to 1, indicating formation of a near-perfectly aligned SAM. Interestingly, in the bulk phase, the value of S remains low up to $\epsilon = 0.065$. This implies that while the molecules prefer to

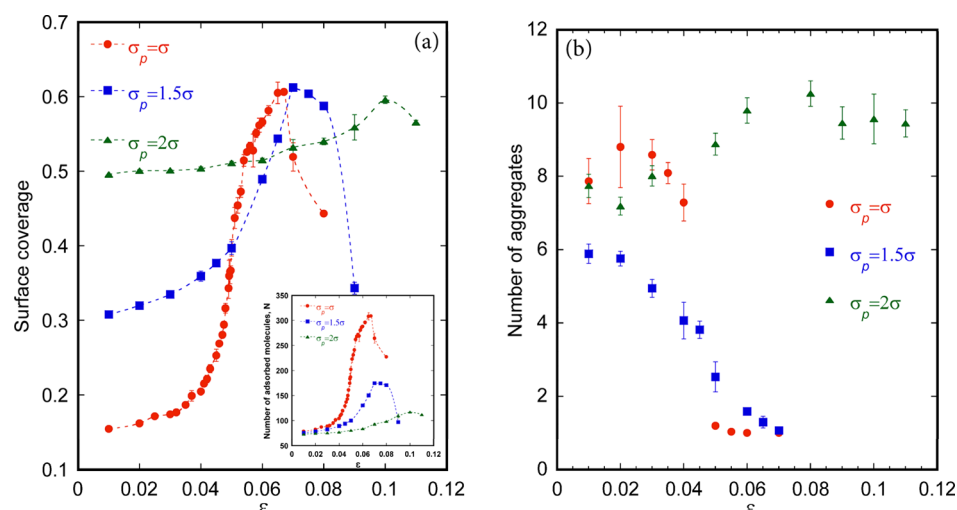


Figure 3. Comparison of adsorption behavior of surfactant molecules with different values of σ_p . (a) Surface coverage (defined in the text) as a function of strength of hydrophobic interactions, ϵ . The inset shows the number of adsorbed molecules, N , for each σ_p as a function of ϵ . (b) Number of aggregates of adsorbed molecules for each σ_p as a function of ϵ . The aggregates are found using the 2D cluster algorithm described in the text.

align parallel to each other in the adsorbed phase for $0.04 < \epsilon < 0.065$ they remain randomly oriented in the bulk phase. Only for $\epsilon > 0.065$ is a sharp increase in the value of S in the bulk phase observed, indicating formation of aggregates or lamellar micelles, which decreases the adsorption, as seen in Figure 1a. It is important to remember that the interaction strength between the polar beads and the surface is kept constant in these simulations. These results show that the adsorption is strongly dependent on tail hydrophobicity and the hydrophobic interactions between surfactant tails promote adsorption and self-assembly on the surface.

Effect of the Size of the Polar Head Group. In the next set of simulations, the size of the polar head bead, σ_p is increased from σ to 1.5σ and 2σ while keeping the size of the hydrophobic beads fixed at $\sigma = 1$. For each value of σ_p , the value of ϵ is varied as before. All other potential parameters are kept fixed.

Adsorbed Amount. To understand the effect of σ_p on the adsorbed amount, one can naively compare the number of adsorbed molecules, N , in each case (Figure 3a inset). However, this comparison will be misleading because with an increase in σ_p the footprint of the molecules adsorbed with their polar bead toward the surface will be larger, and hence, fewer molecules will be expected to get adsorbed. Instead, a fair comparison is to consider the fraction of the surface area covered by the molecules, or surface coverage, for different values of σ_p . The surface coverage is calculated as

$$\text{surface coverage} = \frac{f\pi\sigma_p^2 + (1-f)\pi\sigma^2}{4A} \quad (2)$$

where f is the fraction of adsorbed molecules with their polar head group pointing toward the surface and A is the total surface area.

Figure 3a shows surface coverage for the three values of σ_p as a function of ϵ . The low adsorption regime, observed for $\epsilon < 0.04$ (weakly hydrophobic tails), is dictated by attractive interactions between the polar beads and the surface, which are the same for the three values of σ_p . In this regime, the number of adsorbed molecules is about the same for the three cases (Figure 3a inset), and as a result, the surface coverage is highest

for the largest σ_p . The surface coverage increases with ϵ for the three cases but shows weaker dependence on ϵ as the value of σ_p increases. The maximum surface coverage, while almost invariant of the size of the polar head group, for $\sigma_p = 2\sigma$ is observed at a higher value of ϵ (~ 0.1). Interesting differences in the nature of the adsorbed layer for the three cases explain this observation. Figure 3b shows the number of surface aggregates or 2D clusters observed for the three cases. The methodology to find 2D clusters in the adsorbed phase is similar to one employed previously³⁴ and is briefly described as follows: the monomers that are within a distance of 1.5σ from the surface are projected onto the plane of the surface. The surface is divided into square boxes of length 0.2σ . For each square box, if there exists a monomer whose surface projection is within an in-plane cutoff distance of 0.8 times σ (hydrophobic bead) or σ_p (polar bead) from the center of the square box, then the box is labeled as “occupied” or else is labeled as “vacant”. Adjacent occupied boxes are considered part of one cluster. For $\sigma_p = \sigma$ and 1.5σ , as ϵ increases, the number of surface aggregates decreases and eventually reaches 1, indicating formation of a monolithic adsorbed layer. On the other hand, for $\sigma_p = 2\sigma$, the number of surface aggregates remains large as the ϵ is increased. For this case, as ϵ increases, the adsorbed molecules tend to aggregate into cylindrical micelles (discussed below) and hence do not form a SAM, as seen for smaller values of σ_p . We do not have a good explanation for the observed difference in the number of 2D clusters between the $\sigma_p = \sigma$ and 1.5σ cases for small values of ϵ (< 0.04).

Micelle Formation. To study the nature of aggregation of surfactant molecules in the bulk as well as in the adsorbed phase, we identify clusters of molecules using the density-based spatial clustering of applications with noise (DBSCAN) algorithm.³⁵ This algorithm is useful for finding clusters in a collection of points in space. It works in the following manner: for a point p , if the number of points within a distance r_{cut} is above a cutoff value, N_{cut} then the points are “directly reachable” to the point p . All points that are directly reachable to each other form part of a “cluster”. After identifying the clusters of monomers using the DBSCAN algorithm, we determine the size and the shape of each cluster by finding the

principle eigenvalues of the radius of gyration squared tensor of each cluster. From the principle eigenvalues, the following quantities are defined³⁶

$$\text{Radius of gyration squared, } R_g^2 = \lambda_1 + \lambda_2 + \lambda_3 \quad (3)$$

$$\text{Asphericity, } b = \left[\lambda_1 - \frac{1}{2}(\lambda_2 + \lambda_3) \right] R_g^{-2} \quad (4)$$

$$\text{Acylicity, } c = [\lambda_2 - \lambda_3] R_g^{-2} \quad (5)$$

where λ_i are the eigenvalues and $\lambda_1 > \lambda_2 > \lambda_3$ is the relative magnitude of the three eigenvalues.

A perfectly spherical cluster/micelle will correspond to $b = 0$. Similarly, a perfectly cylindrical cluster will correspond to $c = 0$. However, because even for a spherical cluster the value of c will be close to 0, in order to classify a cluster as cylindrical, one needs to consider asphericity and acylindricity together. Figure 4a shows asphericity and acylindricity of the largest cluster of

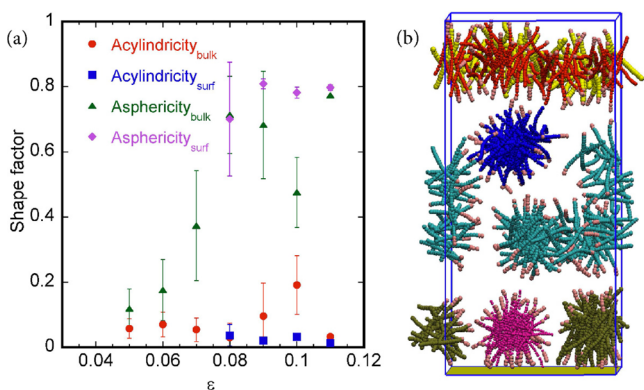


Figure 4. (a) Different shape factors evaluated for the largest cluster identified for molecules with $\sigma_p = 2\sigma$ in the bulk and the adsorbed phase. (b) Snapshot of the simulation system with $\sigma_p = 2\sigma$ and $\epsilon = 0.11$. Different clusters identified by the DBSCAN algorithm are shown via different colors. Cylindrical micelles in the bulk and the adsorbed phases are clearly identifiable.

monomers identified for $\sigma_p = 2\sigma$ for different values of ϵ in the bulk and in the adsorbed phase. In both phases, the acylindricity is small while the asphericity is large, which clearly indicates the formation of cylindrical micelles. While we focus here on only the largest cluster, similar behavior is observed for other clusters as well. Figure 4b shows a snapshot of the system for $\epsilon = 0.11$. One can easily identify distinct cylindrical micelles in both the adsorbed and the bulk phases. For the case of $\sigma_p = 1.5\sigma$, the state of the system is more complicated. For $\sigma_p = 1.5\sigma$, Figure 2Sa,b shows asphericity and acylindricity of the largest cluster in the bulk and the adsorbed phase, respectively (Supporting Information). In both the bulk and the adsorbed phase, the acylindricity and the asphericity are similar in magnitude, thereby demonstrating only a weak tendency of the molecules to form cylindrical micelles. As a result, we are unable to assign a distinct geometrical shape to these clusters (Figure 3S shows one snapshot of the system for $\sigma_p = 1.5\sigma$ and $\epsilon = 0.07$). Note that in Figures 4 and 2S, no data points are shown for small values of ϵ for which no clusters are identified. For the case of $\sigma_p = \sigma$, the orientation factor S shows formation of lamellar micelles in the bulk and the adsorbed phase. Hence, we do not evaluate acylindricity and asphericity shape factors for this case. Observation of lamellar and cylindrical micelles for

the $\sigma_p = \sigma$ and 2σ cases, respectively, can be explained via calculation of the critical packing parameter (CPP).³⁷ CPP is a dimensionless number given by $V/(AL)$, where V is the volume of the tail of the surfactant, A is the area of the surfactant head, and L is the tail length. The CPP is calculated by assuming the tail to be a cylinder with excluded volume, $V = \pi\sigma^2L$, and the polar head excluded area, $A = \pi(\sigma_p + \sigma/2)^2$. For $\sigma_p = \sigma$, $\text{CPP} \approx 1$, which suggests that the molecules will aggregate in lamellar micelles, while for $\sigma_p = 2\sigma$, $\text{CPP} \approx 0.44 < 0.5$, which corresponds to cylindrical micelles.³⁷ From the above results, it is deduced that the adsorbed morphologies depend on the geometry of the surfactant molecules and correspond to bulk aggregation morphologies, a phenomenon that has been observed in AFM studies of adsorption of surfactants on surfaces.³⁸

Nature of the Adsorbed Layer. Figure 5 shows the fraction of adsorbed molecules with their polar head group pointing

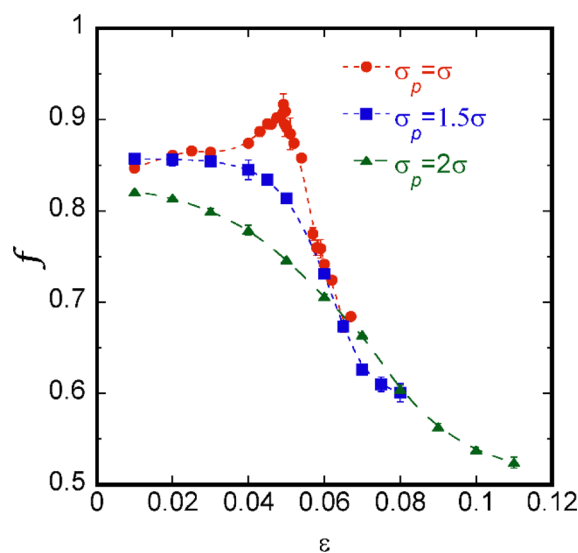


Figure 5. Fraction of the adsorbed surfactant molecules with their polar groups pointing toward the surface, f , as a function of ϵ for different values of σ_p . Lines are guides to the eye.

toward the surface, f , as a function of ϵ for the three values of σ_p . For small values of ϵ (<0.04) corresponding to low adsorption, f is large (>0.8) for all σ_p as this adsorption regime is dominated by the attractive interaction between the polar head groups and the surface. For $\sigma_p = \sigma$, at first f increases with ϵ as the adsorbed molecules start aligning parallel to each other. However, beyond $\epsilon = 0.05$, f decreases with ϵ . The decrease in f is concomitant with the formation of a SAM. The formation of the SAM is dominated by hydrophobic interactions between the tails of the adsorbed molecules, and the polar bead–surface interactions are not significant enough to cause flipping of the adsorbed molecules to have their polar beads toward the surface. Hence, the SAM (at $\epsilon = 0.065$) is patchy with $\sim 30\%$ molecules adsorbed with their polar bead pointing away from the surface. This is an interesting revelation about the nature of the SAM, which is often presumed to form a uniformly hydrophobic layer of adsorbed surfactants.^{4,39} For $\sigma_p = 1.5\sigma$, a monotonic decrease in the f as a function of ϵ is observed. This is a consequence of geometric considerations of efficiently packing molecules with different sized polar and hydrophobic beads on the surface. For $\sigma_p = 2\sigma$ as well, a monotonic decrease

in the f as a function of ε is observed. While for $\sigma_p = 1.5\sigma$ a monolithic adsorbed layer is formed, for $\sigma_p = 2\sigma$, cylindrical micelles form in the adsorbed phase as ε increases, which results in the monotonic decrease in f . Hence, it is observed that the adsorbed layer of surfactant molecules is patchy, with both hydrophobic and polar groups exposed to the solution.

While the focus of this study has been the adsorption of 20mer surfactant molecules, we have also studied the adsorption of 10mer and 30mer surfactant molecules. Because the bond length in our model is 0.3σ , the length to diameter aspect ratio of the 20mer is $l/d \approx 6$, whereas, for the 10mer molecule, $l/d \approx 3$, which we found to be too small to form a stable, adsorbed SAM. Hence, the adsorption behavior of 10mer surfactants is not interesting for the study of self-assembly. On the other hand, 30mer surfactant molecules show similar adsorption behavior as the 20mer surfactant molecules (Figure 4S). From Figure 4S, it is observed that for the 30mer case highest adsorption is achieved at a smaller value of ε ($= 0.046$) as compared to the 20mer case. This is expected as the 30mer molecules will have stronger hydrophobic interactions than the 20mer molecules for the same ε . Furthermore, it is observed that the maximum adsorption for the 30mer molecules (~ 281) is less than that seen for the 20mer molecules (~ 309). We believe that this difference is due to a larger entropy loss associated with the adsorption of the 30mers. We are investigating this aspect in more detail using free energy calculations, and it will be a subject of a future publication.

CONCLUSIONS

Adsorption of surfactant molecules on metal–water interfaces is a useful mechanism for tuning interfacial properties and has found applications in a wide range of fields. The goal of this work is to study how different molecular properties of surfactant molecules affect their adsorption characteristics. From our simulations, we find that tail hydrophobicity plays a significant role in adsorption. When the tail is weakly hydrophobic, only low levels of adsorption are observed even though the polar groups have strong affinity for the surface. For more hydrophobic tails, a SAM in the adsorbed phase is formed. In this regime, adsorption is dominated by hydrophobic interactions between the tails, a phenomenon that has also been reported in experiments.⁴⁰ For surfactants with a larger polar head group than the hydrophobic monomers of the tail, the effect of tail hydrophobicity on surface coverage via adsorption is found to weaken. Nevertheless, the maximum surface coverage is found to be almost invariant of the size of the polar head group. These results explain the experimental observations wherein, for the case of small polar head groups, such as quaternary ammonium derivatives, a dramatic effect of the tail hydrophobicity on adsorption is reported,^{22,26} while for the case of bulky polar groups, such as imidazolium-based groups, adsorption is found to be invariant of the tail hydrophobicity.¹¹ We observe that the adsorbed surfactant layer is patchy, with a good fraction of the polar groups in the adsorbed phase pointing toward the solution. This observation is contrary to the assumption that the adsorbed SAM manifests a uniformly hydrophobic interface to the solution.^{4,39,41} Finally, we find that, in accordance with the experimental observations, the molecules adsorb in micellar structures similar to those observed in the bulk phase.^{18,42} That is, the molecules that have tendency to form cylindrical micelles in the bulk adsorb as cylindrical micelles rather than forming a mono/bilayer. In

experimental studies, the role of tail hydrophobicity is investigated by studying the adsorption behavior of surfactants with different tail lengths. Longer tails are expected to have more conformational entropy loss upon adsorption in comparison to smaller tails. Furthermore, surfactants with longer tails will have different transport and aggregation properties. In this work, we tune the hydrophobic character of surfactant tails while keeping the tail length fixed. This strategy may not have a direct experimental analogue but is useful in isolating the role of hydrophobic interactions from other concomitant effects that arise from varying the alkyl tail length. Similarly, by changing the size of the polar head group without changing its interaction strength with the surface, we study the role of polar group size in isolation of other effects. In summary, this work concludes that the nature of the hydrophobic tail and the polar head group plays an important role in the adsorption characteristics of surfactant molecules, and these factors should be taken into account for rational design of these molecules for different applications.

ASSOCIATED CONTENT

Supporting Information

The Supporting Information is available free of charge on the ACS Publications website at DOI: 10.1021/acs.jpcc.7b09297.

The following figures have been provided as supporting information: Figure 1S: Density profile of center of mass of surfactant molecules as a function of distance from the metal surface, Z for $\sigma_p = \sigma$ and $\varepsilon = 0.065$. Figure 2S: Acylindricity and asphericity of the largest cluster identified for $\sigma_p = 1.5\sigma$ as a function of ε for (a) the bulk phase, and (b) the adsorbed phase. Figure 3S: A snapshot of the simulation system for $\sigma_p = 1.5\sigma$ and $\varepsilon = 0.07$. Figure 4S: The number of adsorbed molecules, N as a function of ε for 20mer and 30mer surfactants with $\sigma_p = \sigma$ (PDF)

AUTHOR INFORMATION

Corresponding Author

*E-mail: sharmas@ohio.edu.

ORCID

Xueying Ko: 0000-0002-7744-7690

Sumit Sharma: 0000-0003-3138-5487

Notes

The authors declare no competing financial interest.

ACKNOWLEDGMENTS

Acknowledgement is made to the donors of the American Chemical Society Petroleum Research Fund (ACS PRF number: 56892-DNI6) for support of this research. This work is partially supported by the NSF CBET Grant 1705817. The authors thank researchers at the Institute of Corrosion and Multiphase Technology (ICMT) for useful discussions. Computational resources for this work were provided by the Ohio Supercomputer Center.

REFERENCES

- (1) Somorjai, G. A.; Li, Y. *Introduction to Surface Chemistry and Catalysis*; John Wiley & Sons: Hoboken, NJ, 2010.
- (2) *Modern Aspects of Electrochemistry*, Number 38; Conway, B. E., Ed.; Springer Science & Business Media: New York, 2005.

- (3) Finšgar, M.; Jackson, J. Application of Corrosion Inhibitors for Steels in Acidic Media for the Oil and Gas Industry: A Review. *Corros. Sci.* **2014**, *86*, 17–41.
- (4) Li, J.; Kaifer, A. E. Surfactant Monolayers on Electrode Surfaces: Self-Assembly of a Viologen Derivative Having a Cholesteryl Hydrophobic Residue. *Langmuir* **1993**, *9*, 591–596.
- (5) Naik, R. R.; Stringer, S. J.; Agarwal, G.; Jones, S. E.; Stone, M. O. Biomimetic Synthesis and Patterning of Silver Nanoparticles. *Nat. Mater.* **2002**, *1*, 169–172.
- (6) Wang, X.; Hsing, I.-M. Surfactant Stabilized Pt and Pt Alloy Electrocatalyst for Polymer Electrolyte Fuel Cells. *Electrochim. Acta* **2002**, *47*, 2981–2987.
- (7) Zhang, J.; Li, C. M. Nanoporous Metals: Fabrication Strategies and Advanced Electrochemical Applications in Catalysis, Sensing and Energy Systems. *Chem. Soc. Rev.* **2012**, *41*, 7016–7031.
- (8) McMahon, A. J. The Mechanism of Action of an Oleic Imidazoline Based Corrosion Inhibitor for Oilfield Use. *Colloids Surf.* **1991**, *59*, 187–208.
- (9) Martin, J. A.; Valone, F. W. The Existence of Imidazoline Corrosion Inhibitors. *Corrosion* **1985**, *41*, 281–287.
- (10) Duda, Y.; Govea-Rueda, R.; Galicia, M.; Beltran, H. I.; Zamudio-Rivera, L. S. Corrosion Inhibitors: Design, Performance, and Computer Simulations. *J. Phys. Chem. B* **2005**, *109*, 22674–22684.
- (11) Edwards, A.; Osborne, C.; Webster, S.; Klenerman, D.; Joseph, M.; Ostovar, P.; Doyle, M. Mechanistic Studies of the Corrosion Inhibitor Oleic Imidazoline. *Corros. Sci.* **1994**, *36*, 315–325.
- (12) Tan, Y.-J.; Bailey, S.; Kinsella, B. An Investigation of the Formation and Destruction of Corrosion Inhibitor Films Using Electrochemical Impedance Spectroscopy (EIS). *Corros. Sci.* **1996**, *38*, 1545–1561.
- (13) Nestic, S.; Wilhelmsen, W.; Skjerve, S.; Hesjektivik, S. M. Testing of Inhibitors for CO₂ Corrosion Using the Electrochemical Techniques. *Proceedings of the 8th European Symposium on Corrosion Inhibitors*, Ann. Univ. Ferrara, NS, Sez. V, Suppl, Ferrara, Italy; Università di Ferrara, 1995; pp 1163–1192.
- (14) Gece, G. Drugs: A Review of Promising Novel Corrosion Inhibitors. *Corros. Sci.* **2011**, *53*, 3873–3898.
- (15) Raja, P. B.; Sethuraman, M. G. Natural Products as Corrosion Inhibitor for Metals in Corrosive Media—a Review. *Mater. Lett.* **2008**, *62*, 113–116.
- (16) Gece, G.; Bilgiç, S. A Theoretical Study on the Inhibition Efficiencies of Some Amino Acids as Corrosion Inhibitors of Nickel. *Corros. Sci.* **2010**, *52*, 3435–3443.
- (17) Jovancevic, V.; Ramachandran, S.; Prince, P. Inhibition of Carbon Dioxide Corrosion of Mild Steel by Imidazolines and Their Precursors. *Corrosion* **1999**, *55*, 449–455.
- (18) Manne, S.; Cleveland, J. P.; Gaub, H. E.; Stucky, G. D.; Hansma, P. K. Direct Visualization of Surfactant Hemimicelles by Force Microscopy of the Electrical Double Layer. *Langmuir* **1994**, *10*, 4409–4413.
- (19) Goloub, T. P.; Koopal, L. K.; Bijsterbosch, B. H.; Sidorova, M. P. Adsorption of Cationic Surfactants on Silica. Surface Charge Effects. *Langmuir* **1996**, *12*, 3188–3194.
- (20) Patrick, H. N.; Warr, G. G.; Manne, S.; Aksay, I. A. Self-Assembly Structures of Nonionic Surfactants at Graphite/Solution Interfaces. *Langmuir* **1997**, *13*, 4349–4356.
- (21) Somasundaran, P.; Fuerstenau, D. W. Mechanisms of Alkyl Sulfonate Adsorption at the Alumina-Water Interface. *J. Phys. Chem.* **1966**, *70*, 90–96.
- (22) Fan, A.; Somasundaran, P.; Turro, N. J. Adsorption of Alkyltrimethylammonium Bromides on Negatively Charged Alumina. *Langmuir* **1997**, *13*, 506–510.
- (23) Patrick, H. N.; Warr, G. G.; Manne, S.; Aksay, I. A. Surface Micellization Patterns of Quaternary Ammonium Surfactants on Mica. *Langmuir* **1999**, *15*, 1685–1692.
- (24) Jaschke, M.; Butt, H.-J.; Gaub, H. E.; Manne, S. Surfactant Aggregates at a Metal Surface. *Langmuir* **1997**, *13*, 1381–1384.
- (25) Atkin, R.; Craig, V. S. J.; Wanless, E. J.; Biggs, S. The Influence of Chain Length and Electrolyte on the Adsorption Kinetics of Cationic Surfactants at the Silica–Aqueous Solution Interface. *J. Colloid Interface Sci.* **2003**, *266*, 236–244.
- (26) Goloub, T. P.; Koopal, L. K. Adsorption of Cationic Surfactants on Silica. Comparison of Experiment and Theory. *Langmuir* **1997**, *13*, 673–681.
- (27) Allen, M. P.; Tildesley, D. J. *Computer Simulation of Liquids*; Oxford University Press: New York, 1989.
- (28) Weeks, J. D.; Chandler, D.; Andersen, H. C. Role of Repulsive Forces in Determining the Equilibrium Structure of Simple Liquids. *J. Chem. Phys.* **1971**, *54*, 5237–5247.
- (29) Van Oss, C. J.; Chaudhury, M. K.; Good, R. J. Interfacial Lifshitz-Van Der Waals and Polar Interactions in Macroscopic Systems. *Chem. Rev.* **1988**, *88*, 927–941.
- (30) Choudhury, N.; Pettitt, B. M. On the Mechanism of Hydrophobic Association of Nanoscopic Solutes. *J. Am. Chem. Soc.* **2005**, *127*, 3556–3567.
- (31) Kovačević, N.; Milošev, I.; Kokalj, A. How Relevant Is the Adsorption Bonding of Imidazoles and Triazoles for Their Corrosion Inhibition of Copper? *Corros. Sci.* **2017**, *124*, 25.
- (32) Plimpton, S. Fast Parallel Algorithms for Short-Range Molecular Dynamics. *J. Comput. Phys.* **1995**, *117*, 1–19.
- (33) Padmanabhan, V.; Kumar, S. K.; Yethiraj, A. Phase Behavior of Semiflexible Polymer Chains. *J. Chem. Phys.* **2008**, *128*, 124908.
- (34) Sharma, S.; Debenedetti, P. G. Free Energy Barriers to Evaporation of Water in Hydrophobic Confinement. *J. Phys. Chem. B* **2012**, *116*, 13282–13289.
- (35) Ester, M.; Kriegel, H.-P.; Sander, J.; Xu, X. A Density-Based Algorithm for Discovering Clusters in Large Spatial Databases with Noise. In *Proceedings of the Second International Conference on Knowledge Discovery and Data Mining*, Portland, OR; Simoudis, E.; Han, J.; Fayyad, U., Eds.; AAAI Press: Menlo Park, CA, 1996; pp 226–231.
- (36) Arkin, H.; Janke, W. Gyration Tensor Based Analysis of the Shapes of Polymer Chains in an Attractive Spherical Cage. *J. Chem. Phys.* **2013**, *138*, 054904.
- (37) Abbott, S. Surfactant Science: Principles and Practice, Creative commons, 2015. <http://www.stevenabbott.co.uk/practical-surfactants/the-book.php> (accessed Sept 8, 2017).
- (38) Atkin, R.; Craig, V. S. J.; Wanless, E. J.; Biggs, S. Mechanism of Cationic Surfactant Adsorption at the Solid–Aqueous Interface. *Adv. Colloid Interface Sci.* **2003**, *103*, 219–304.
- (39) Xiong, Y.; Brown, B.; Kinsella, B.; Nešić, S.; Pailleret, A. Atomic Force Microscopy Study of the Adsorption of Surfactant Corrosion Inhibitor Films. *Corrosion* **2014**, *70*, 247–260.
- (40) Rupperecht, H.; Gu, T. Structure of Adsorption Layers of Ionic Surfactants at the Solid/Liquid Interface. *Colloid Polym. Sci.* **1991**, *269*, 506–522.
- (41) Ramachandran, S.; Tsai, B.-L.; Blanco, M.; Chen, H.; Tang, Y.; Goddard, W. A. Self-Assembled Monolayer Mechanism for Corrosion Inhibition of Iron by Imidazolines. *Langmuir* **1996**, *12*, 6419–6428.
- (42) Manne, S.; Schäffer, T. E.; Huo, Q.; Hansma, P. K.; Morse, D. E.; Stucky, G. D.; Aksay, I. A. Gemini Surfactants at Solid–Liquid Interfaces: Control of Interfacial Aggregate Geometry. *Langmuir* **1997**, *13*, 6382–6387.